

KINEMATICS AND DYNAMICS OF THE H II REGION SHARPLESS 142.  
I. THE VELOCITY FIELD OF THE IONIZED HYDROGEN

GILLES JONCAS AND JEAN-RENÉ ROY

Département de physique, Observatoire astronomique du mont Mégantic, Université Laval

Received 1983 December 19; accepted 1984 February 29

## ABSTRACT

Fabry-Perot interferometry at H $\alpha$  and efficient image processing techniques have allowed the measurement of nearly 41,000 radial velocities across the H II region S142. The mean  $V_{\text{LSR}}$  is  $-35.6 \pm 0.1 \text{ km s}^{-1}$ , and the standard deviation of the velocity distribution is  $12.5 \text{ km s}^{-1}$ ; this corresponds to a redshift of  $+5 \text{ km s}^{-1}$  with respect to the associated molecular cloud observed by Israel east of the nebula. S142 is ionization bounded on the eastern side while the western side appears density bounded; the H II region and its associated complex of neutral material are seen roughly edge-on. Maps of radial velocities were constructed by taking the average value of all velocities measured in each  $1' \times 1'$  window across the H II region. The observed H $\alpha$  velocity field is interpreted as a systematic expansion of the ionized gas; a velocity gradient in the plane of the sky of  $\sim 1.1 \text{ km s}^{-1} \text{ pc}^{-1}$  is observed away from the hot component of the molecular cloud. The locus of the most negative H $\alpha$  velocities ( $V_{\text{LSR}} \approx -50 \text{ km s}^{-1}$ ) coincides with the position of the hot component of the molecular cloud and with the zones of strongest 21 cm continuum emission. There is a striking match between the most negative H $\alpha$  velocities and the shape of the  $^{12}\text{CO}$  emission contours of the nebular side. The terminal H $\alpha$  velocities found in the northern, western, and southwestern sections of S142 reach about  $35 \text{ km s}^{-1}$  with respect to the reference  $V_{\text{LSR}}$  of the molecular cloud. The dispersions of H $\alpha$  velocities from the mean for each  $1' \times 1'$  window have a most probable value of  $7 \text{ km s}^{-1}$ . Several features of the morphology and of the observed kinematics of S142 are in close agreement with the predictions of the "champagne" model of Tenorio-Tagle.

*Subject headings:* interferometry — nebulae: H II regions — nebulae: individual — radial velocities

## I. INTRODUCTION

Most diffuse nebulae are objects of very low surface brightness. Consequently, high spectral resolution with sufficient signal-to-noise ratio, needed to measure radial velocities across their surface, is difficult to achieve. With the exception of a few investigations done with multislit spectrographs on the brightest nebulae (e.g., Wilson *et al.* 1959 on M42; Mufson *et al.* 1981 on M16; Fountain, Gary, and O'Dell 1979, 1983 on the Rosette nebula and on NGC 1499, NGC 7000, and IC 1318 b/c), the kinematics of H II regions has been studied mainly by Fabry-Pérot (F-P) interferometry, because of the high luminosity-resolution product of such a device and of its great efficiency and contrast when combined with fast optical systems (Courtès 1972; Atherton *et al.* 1982). Despite the large number of nebulae investigated since the 1960s, very few studies have provided velocity maps detailed enough to be matched with the most evolved dynamical models, such as the "champagne" model proposed by Tenorio-Tagle (1979). On the other hand, most, if not all, diffuse nebulae are linked in some way to parent clouds of neutral and molecular gas. Thus, combining observations of the molecular, neutral, and ionized gas can only lead to a better understanding of the interaction between nebulae and their neutral environment and of their respective evolution. Except for general surveys and compilations (Israel 1978; Blitz, Fich, and Stark 1982; Deharveng 1980), only a few researchers have used this complementary approach.

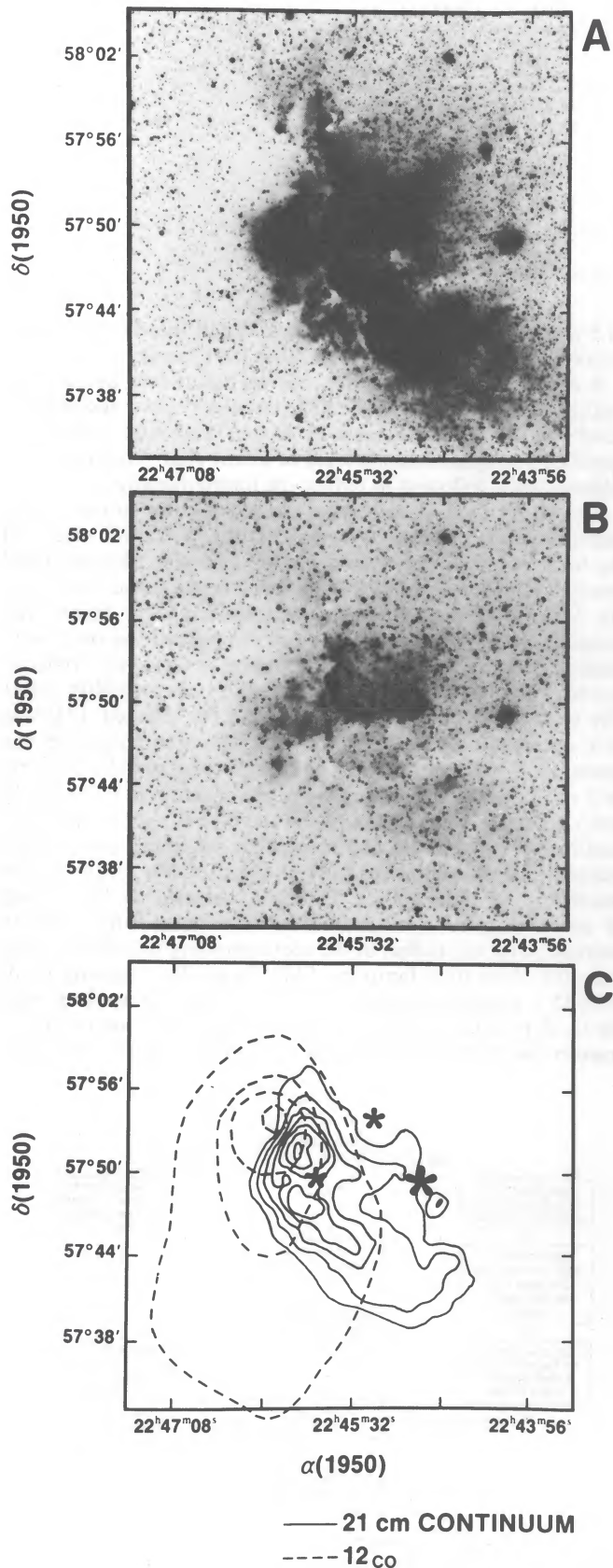
This state of things has recently been improved by the use of scanning and servo-stabilized F-P interferometers, better detectors, more efficient techniques for the reduction of interferograms, and radio synthesis interferometers equipped with

high-resolution spectrometers. With such tools in hand, we have completed a detailed kinematic study of the neutral and ionized hydrogen of the H II region S142 and its surroundings.

This paper deals mainly with the optical results obtained by F-P interferometry at H $\alpha$ . A brief description of our F-P camera and of the software developed for the reduction of digitized interferograms is also given; a more elaborate discussion has been published elsewhere (Joncas 1983; Joncas and Roy 1984). Our approach has allowed us to sample extensively the observed field of view, leading to a dramatic increase in the number of velocity points one can measure on each interferogram. A forthcoming paper will describe the radio observations (continuum and line at 21 cm) obtained with a  $1' \times 1/2'$  resolution at the Dominion Radio Astrophysical Observatory.

## II. BACKGROUND ON S142

The H II region S142 [ $\alpha(1950) = 22^{\text{h}}45^{\text{m}}36^{\text{s}}$ ,  $\delta(1950) = 57^{\circ}48'$ ], contains the open star cluster NGC 7380 which is  $2\text{--}3 \times 10^6$  years old (Moffat 1971). This large and relatively bright nebula is located in the Perseus arm ( $l = 107.14$ ,  $b = -0.96$ ) at  $\sim 3.5$  kpc from the Sun (Moffat 1971; Humphreys 1978). Figure 1 presents a composite illustration summarizing various aspects of the nebula. On the red print of the POSS, S142 shows an intriguing morphology of superposed half-shells which are probably the result of the interaction of ionization fronts (IF) with neutral clouds. The northern, western, and southern frontiers are faint and ill defined; the nebula is probably density limited on those sides. The eastern and southern frontiers are well defined; a parent cloud of neutral gas is most likely present, making the nebula ionization bounded on that side.



The principal ionizing star is HD 215835, also known as DH Cep (Hiltner 1956), which is a spectroscopic binary located in the western portion of the nebula; both components are O6 stars (Goy 1973) of luminosity class I (Andrews 1968) or V (Humphreys 1978). Israel (1977) has suggested that two other stars (spectral types O9 and O9.5) may also contribute to the ionization (Fig. 3). From radio observations, Felli and Harten (1981) have calculated that  $2.45 \times 10^{49}$  photons  $s^{-1}$  are necessary to ionize S142. HD 215835 emits at least  $3.5 \times 10^{49}$  photons  $s^{-1}$  (Panagia 1973), plainly enough to ionize the nebula by itself.

Local standard of rest (LSR) radial velocity measurements in H $\alpha$  of S142 have been made by Courtès *et al.* (1966) [ $-35.4$  km  $s^{-1}$ ], Williamson (1970) [ $-41.0$  km  $s^{-1}$ ], Georgelin and Georgelin (1970) [ $-35.8$  km  $s^{-1}$ ], and Crampton, Georgelin, and Georgelin (1978) [ $-45.3$  km  $s^{-1}$ ], using a F-P etalon, and Miller (1968) [ $-45.3$  km  $s^{-1}$ ] with a spectrograph. The measurements differ from one author to the other, probably due to the small number or velocity points (actually  $\leq 65$ ) observed in different parts of the nebula.

Radio observations of S142 have been made in the continuum by Israel (1977) and Felli *et al.* (1977, 1978) and in the recombination lines of hydrogen by Pedlar (1980) and Garay and Rodríguez (1983). A summary of these observations is given in Table 1. The nebula appears to be a relatively old H II region: no fine details are apparent in the continuum maps; the mean electron density is around  $25$   $cm^{-3}$ . The similarity between the morphology of the nebula on the red print of the POSS and the radio continuum map (Fig. 1a, c) indicates rather uniform extinction over that region. Moffat (1971) has deduced a mean visual extinction  $\sim 1.9$  mag for 55 stars of the cluster NGC 7380. East of S142, Israel (1980) observed a molecular cloud (Fig. 1), smaller than the ionized cloud, associated with the nebula; the extent of the CO cloud is  $\sim 7$  pc, its mass  $\sim 200 M_{\odot}$  and density ( $H_2$ )  $\sim 60$   $cm^{-3}$ . The core of this cloud has two components: one ( $V_{LSR} = -41.1$   $s^{-1}$ ) is dense, while the other ( $-42.8$   $km s^{-1}$ ) is hot and less dense (Table 1). No OH/H $_2$ O maser sources has been detected so far. Therefore, very little star formation activity, if any at all, is occurring in S142. The hotter component of the molecular cloud may thus be an externally heated globule in the process of disintegration (Israel 1980).

## II. OBSERVATIONS AND DATA PROCESSING

### a) The Instrument

The F-P camera that we have built combines a focal reducer, its guiding head, and a servo-stabilized scanning F-P interferometer. The focal reducer ( $f/8 \rightarrow f/0.95$ ) uses a collimator lens of 80.6 mm in diameter, with its peak efficiency in the H $\alpha$  and He I 1083.0 nm domain, and a 25 mm ( $f/0.95$ ) Angénieux camera lens (circle of least confusion of 25  $\mu m$ ). At the Ritchey-Chrétien  $f/8$  focus of the 1.6 m telescope of the Observatoire astronomique du mont Mégantic, this lens gives a spatial resolution of 3". An H $\alpha$  filter ( $\Delta\lambda \approx 1.0$  nm and  $d = 50$  mm) is used as a premonochromator and sets the field of view at  $\sim 14'$ .

FIG. 1.—Red (A) and blue (B) prints of the Palomar Observatory Sky Survey (POSS) showing S142 and its surroundings. Maps (C) of the same region showing the 21 cm continuum radio emission and of the velocity integrated ( $-10$  to  $-59$   $km s^{-1}$ )  $^{12}CO$  intensity. The CO map (from Israel 1980) was obtained with a half-power beamwidth of  $2.3$ ; contours are in step of 2.6  $km s^{-1}$ . The asterisks represent the three O stars exciting S142, with the largest symbol for DH Cep.

TABLE 1  
SUMMARY OF RADIO RECOMBINATION LINE AND MOLECULAR OBSERVATIONS

Frequency (MHz)	$V_{\text{LSR}}$ (km s $^{-1}$ )	FWHM (km s $^{-1}$ )	$T_e$ (K)	Authors
1425 (H166 $\alpha$ ) .....	$-43.0 \pm 2.0$	25.5	4900	Pedlar 1980
3331 (H125 $\alpha$ ) .....	$-37.2 \pm 0.5$	$25.6 \pm 1.3$	$7700 \pm 600$	Garay and Rodriguez 1983
3331 (H158 $\beta$ ) .....	$-36.2 \pm 1.5$	$28.2 \pm 3.5$	...	Garay and Rodriguez 1983
11500 ( $^{12}\text{CO}$ ) .....	$-42.8 \pm 0.7$	$2.7 \pm 0.7$	...	Israel 1980
11500 ( $^{13}\text{CO}$ ) .....	$-41.1 \pm 0.7$	$1.5 \pm 0.7$	...	Israel 1980
11500 ( $^{12}\text{CO}$ ) .....	$-41.0 \pm 0.5$	$2.7 \pm 0.7$	...	Blitz <i>et al.</i> 1982

The detector is a IIIa-F photographic plate. The scanning F-P interferometer (spacing  $\sim 348 \mu\text{m}$  and reflectivity = 82%) has a FWHM of 0.044 nm (20.1 km s $^{-1}$ ) and a free spectral range of 0.62 nm at H $\alpha$ , and is optimized to operate between 600.0 and 700.0 nm.

When the F-P is introduced into the focal reducer, the image of the source is modulated by the interference pattern of the interferometer. Transmission maxima occur at  $m\lambda = 2\mu t \cos \theta$ , where  $\mu$  is the refraction index of the interferometer gap,  $t$  the interferometer spacing,  $\theta$  the incidence angle with respect to the normal of the F-P,  $m$  the order of interference, and  $\lambda$  the wavelength. Thus, if the brightness of the source is uniform, the resulting pattern is a series of concentric rings corresponding to successive orders of interference. The Doppler effect modifies the wavelength of a spectral "ring" in such a way that the radius,  $R_{\text{OBS}}$ , of the observed fringe differs from the radius,  $R_m$ , of the calibration source ring by an amount related to the radial velocity,  $v$ , such as

$$v = \frac{c}{2F_{\text{CAM}}} (R_m^2 - R_{\text{OBS}}^2), \quad (1)$$

where  $F_{\text{CAM}}$  is the equivalent focal length of the focal reducer camera lens and  $c$  the velocity of light.

#### b) The Observations

The observations were made at the f/8 Ritchey-Chrétien focus of the Observatoire astronomique de mont Mégantic 1.60 m telescope. In addition to H $\alpha$  and [O III] 500.7 nm filtergrams, 13 H $\alpha$  interferograms of 3 hours exposure each were analyzed, covering S142 almost entirely. This coverage was achieved by dividing the nebula (diameter of  $\sim 25'$ ) into six overlapping sections, to enable extensive velocity checks; by setting the interferometer at different spacings, the field of each nebular section was thus "scanned." Comparison interferograms from a hydrogen calibration lamp were also obtained to calculate the nebular radial velocity (eq. [1]); these were taken before and after each exposure of S142 to check the stability of the interferometer. Possible drifts of the servo-stabilized etalon were monitored by comparing the before and after radii of the calibration rings. Over a period of a few hours, the separation of the F-P plates does not change by more than 2.5 nm, which correspond to a wavelength drift of 0.005 nm, i.e., 2 km s $^{-1}$ . Interferograms for which the drift was larger than this were rejected. Larger drifts were caused by insufficient time given to the electronics to stabilize.

#### c) Data Handling

The photographic plates were digitized with the PDS microdensitometer of David Dunlap Observatory. A square slit of

12.5  $\mu\text{m}$  was used with 10  $\mu\text{m}$  steps. Each interferogram was thus converted into a matrix of 760  $\times$  1001 pixels.

A complete set of software was elaborated to analyze the digitized interferograms. The different algorithms, described in detail in Joncas (1983) and in Joncas and Roy (1984), are sketched in Figure 2 in the form of a flow chart identifying the different steps followed to reduce the interferograms.

The slight spatial distortion caused by the optics of the instrument was calibrated by means of a X-Y grid placed at the focal plane of the telescope. The grid was photographed through the focal reducer and digitized in the same way as the H $\alpha$  interferograms. With the distortion effects taken into account, the center and the radii of the calibration rings were measured using an algorithm applying connectivity rules to locate the rings in the image matrix (Joncas and Roy 1984). The equivalent focal length of the camera lens (eq. [1]) was then obtained from the radii of the calibration rings after the method of Born and Wolf (1975). The local nebular velocity field modifies the shape and the position of the F-P fringes. In order to establish the radii of the nebular fringes, the density maxima were identified and located by searching along radial vectors (density versus radius) starting at the center of the interferogram of the nebula. The radial velocity can be deduced by comparing the local radius of the nebular fringe (density maxima) with the radius of the corresponding interference ring from the calibration lamp (eq. [1]). To produce velocity maps of S142, a program originating from NRAO was applied using the ( $\alpha$ ,  $\delta$ ) positions of 79 stars distributed across the nebula to convert the PDS coordinates of the velocity points into equa-

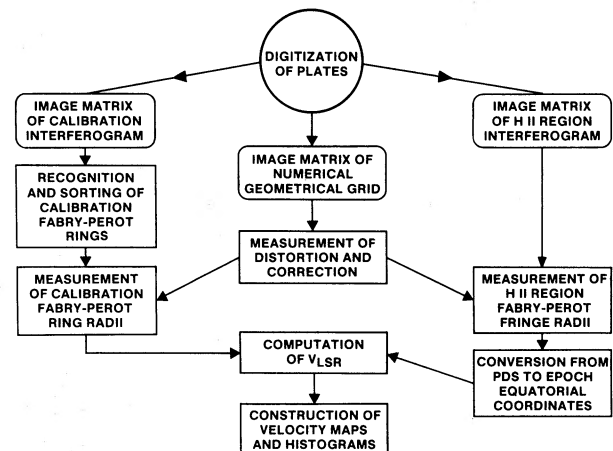


FIG. 2.—Flow chart summarizing the successive steps followed in processing the Fabry-Pérot photographic interferograms. Conversion into LSR velocities was done following the equations presented in Lang (1980).

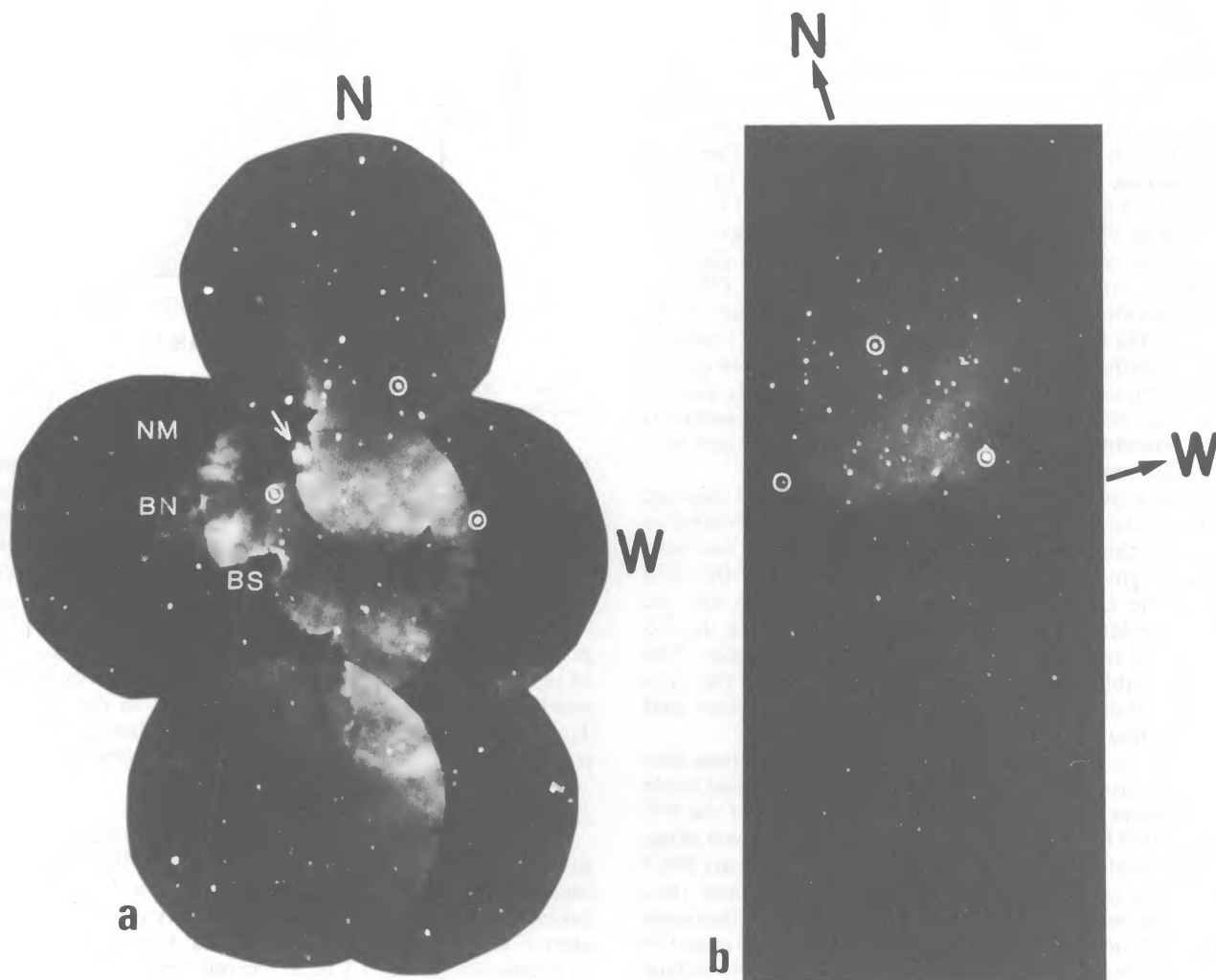


FIG. 3.—Mosaics of (a)  $H\alpha$  and (b)  $[O\ III] 500.7\text{ nm}$  photographs of S142 obtained with a  $f/8 \rightarrow f/0.95$  focal reducer at the Mount Mégantic Observatory 1.60 m telescope. The exciting stars are circled, with DH Cep, the main ionizing source, being the westernmost star, then the northern O9.5 star and the eastern O9 star. The  $H\alpha$  knot (LS 57:89) is identified by an arrow, and NM locates the centroid of the  $^{12}\text{CO}$  molecular cloud. BN and BS are for the northern and southern bright rims. Notice the slightly different orientations of the two mosaics.

torial epoch coordinates. Each interferogram contained at least 10 stars, thus allowing accurate conversions.

### III. MORPHOLOGY AND IONIZATION STRUCTURE OF S142

The photography of nebulae, using narrow bandpass filters centered on their emission lines, can lead to important information on the properties of H II regions. The study of lines emitted from ions having different ionization potentials and ionization degrees enables to determine the ionization structure of the nebula. For S142, only H $\alpha$  and [O III] 500.7 nm plates were obtained; exposure time for the other lines (e.g., H $\beta$ , [N II]) would have been prohibitively long (Hawley 1978).

Figure 3 presents a mosaic in H $\alpha$  of S142. The three stars most likely to contribute to the ionization of the nebula are encircled. The westernmost star is HD 215835(DH Cep), the O6 spectroscopic binary. S142 is divided in two parts by a lane of decreased H $\alpha$  emission. Each part contains at least one star contributing to the ionization. In the eastern part, two bright rims are clearly seen. Their geometry and brightness distribution seem to indicate that the progenitor is the O9 star described previously (Pottach 1958). To the northwest of the O9 star is an H $\alpha$  knot which coincides with the early type star LS 57 $^{\circ}$ 89 (identified by an arrow in Fig. 3). The western part of the nebula is much more homogeneous; it is probably density bounded. The difference in brightness between the southern and southwestern plates of the mosaic is artificial and was caused by different exposure times.

To complete our [O III] 500.7 nm observations, we used the blue POSS plate of S142. The nebula is once again divided in two parts but this time along an east-west axis. The northern part is the brightest; it encompasses the majority of the stars composing the cluster NGC 7380. This separation may be caused by the lane of decreased ionization found in the H $\alpha$  plates. The [O III] 500.7 nm emission is homogeneous. The bright knot visible at H $\alpha$  does not appear in [O III]; this type of object is known to be of low excitation (Chopin et al. and Lortet-Zuckermann 1972).

To explain the ionization structure of S142, we propose that the dark lane cutting S142 is a sheet viewed edge-on and made up of a sufficient amount of dust to prevent some of the UV photons emitted by HD 215835 from reaching every part of the nebula; this would explain the low intensity of the [O III] 500.7 nm line in the southern part of the nebula. This sheet rises upward to the north (Fig. 3), also depriving the northeastern section of S142 of some UV photons; but the presence of an O9 star compensates for this deficiency, since the northeastern section has a higher blue emissivity (POSS plate) than the southern section. We mentioned earlier that the source of ionizing photons for the bright rims seems to be the O9 star; however, their geometry does not totally exclude the participation of HD 215835. The number of ionizing photons ( $\sim 3.5 \times 10^{49}$  photons  $s^{-1}$ ) emitted by this star is so high that we cannot disregard them wherever we are in the nebula.

### IV. THE H $\alpha$ VELOCITY FIELD OF S142

#### a) Histogram of the LSR Velocity Points

The histogram of all the velocity points (40,983) measured on S142 is shown in Figure 4. The mean LSR velocity is  $-35.6 \pm 0.1$  km  $s^{-1}$ . The best optical and radio observations (Georgelin and Georgelin 1970; Garay and Rodríguez 1983) are in excellent agreement with this result. The standard deviation of the H $\alpha$  LSR velocities is 12.5 km  $s^{-1}$ . This value is

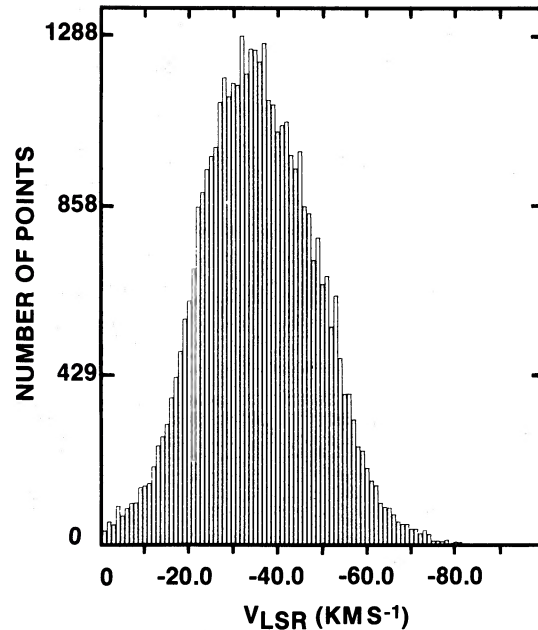


FIG. 4.—Histogram of the 40983  $V_{\text{LSR}}$  measured at H $\alpha$  across S142. The mean is  $-35.6 \pm 0.1$  km  $s^{-1}$  with a standard deviation of 12.5 km  $s^{-1}$ .

large for a galactic H II region but is not unexpected considering the size ( $\sim 25$  pc) of S142. Notice that this “dispersion” does not correspond mathematically to the usual velocity dispersion or turbulence measured from the  $e$ -folding width deduced from line profiles. We will come back to this subject in § IVc. The  $V_{\text{LSR}}$  histogram has a Gaussian distribution; its skewness is  $-0.075$ . However, it should be remarked that some of the individual histograms corresponding to various sections of the nebula deviate from a Gaussian. The mean H $\alpha$   $V_{\text{LSR}}$  is redshifted by  $\sim +5$  km  $s^{-1}$  with respect to the CO cloud’s  $V_{\text{LSR}}$ , which indicates that most of the ionized gas is rushing away from the molecular cloud and from the observer.

#### b) The H $\alpha$ Velocity Maps

The large number of velocity points measured enables us to present extremely detailed and thorough H $\alpha$  velocity field maps. The maps were constructed with a  $1'$  resolution by taking the average value of all the velocity points contained in each  $1' \times 1'$  window across the nebula; this scale corresponds to a smoothing over 1.1 pc at the inferred distance of 3.5 kpc. The gain in statistical weight is not at the cost of spatial resolution, since maps drawn with  $30''$  resolution did not reveal more meaningful small-scale movements in S142.

The LSR velocity maps are shown with 7 km  $s^{-1}$  steps in Figure 5. The differing symbols indicate the number of velocity points which were averaged in every  $1' \times 1'$  window; they are defined in Table 2. Little weight must thus be given to data points having symbol A. The most striking feature is the gradient in velocity across the nebula. The less negative velocities ( $\sim -15$  km  $s^{-1}$ ) are located in the western and in the northern sections of S142, i.e., the density-bounded edge. The more negative velocities ( $\sim -50$  km  $s^{-1}$ ) are found at the northeastern section, close to the molecular cloud ( $V_{\text{LSR}} = -41$  km  $s^{-1}$ ) and coincides with the zones of highest radio continuum (Fig. 6). The match between the velocity structure of the ionized hydrogen and the contour of CO emission is indeed eloquent. The velocity of the ionized gas which flows out from

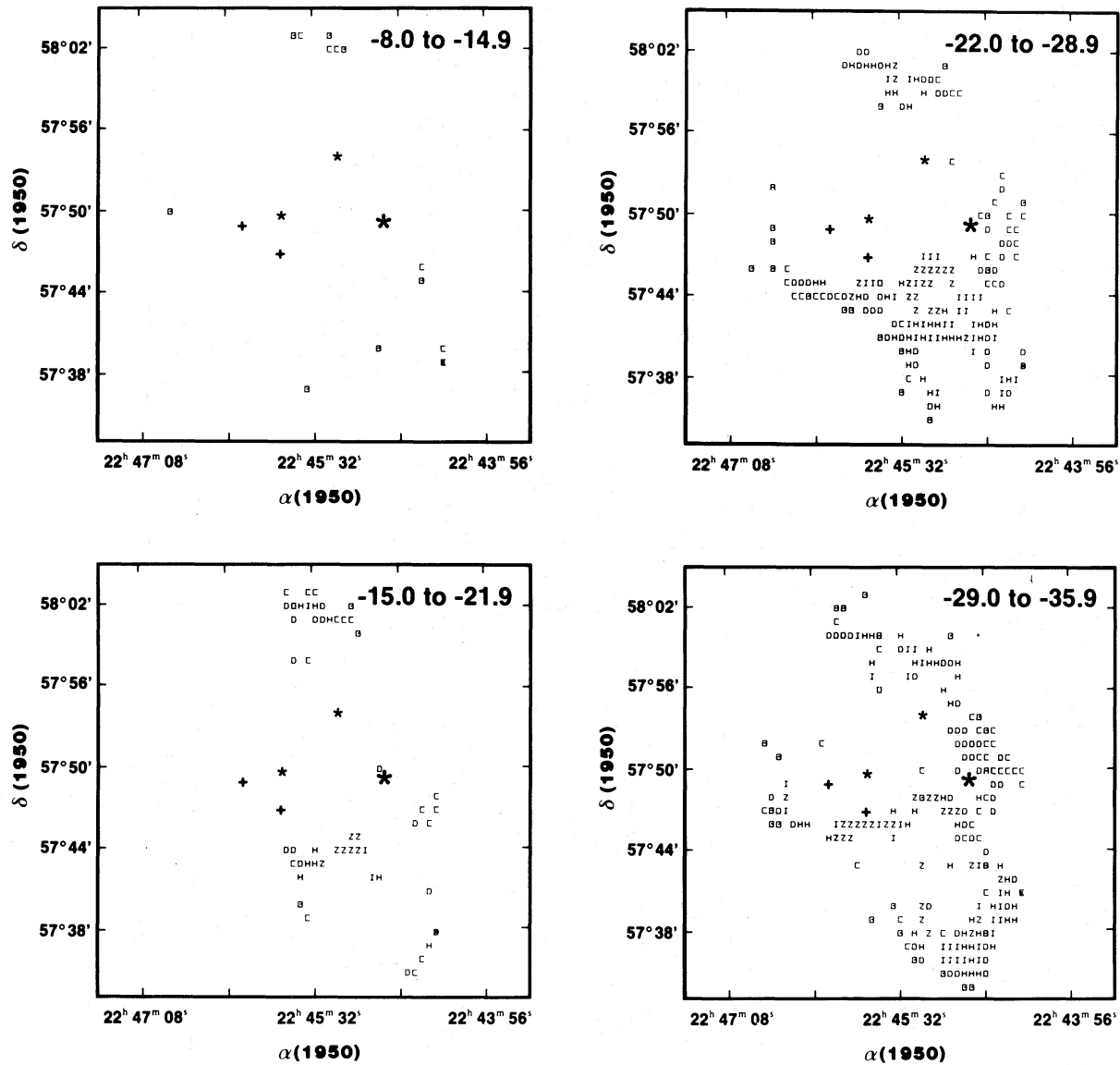


FIG. 5a

FIG. 5.—(a) H $\alpha$  LSR velocity maps of S142 in steps of 7 km s<sup>-1</sup> averaged over 1'. The different letters represent the number of velocity points averaged over each 1' x 1' window; their values are listed in Table 2. The asterisks represent the three O stars exciting S142, with the largest symbol for DH Cep. The crosses indicate the position of the bright rims marked as BN and BS in Fig. 3. (b) Gray-scale representation of the velocity field shown in Fig. 5a. Lighter shades correspond to the more negative velocities. The full line is the outer contour of 21 cm continuum emission.

the northern bright rim (Fig. 3) varies from -50.0 to -56.9 km s<sup>-1</sup> (Fig. 5). At the southern bright rim (Fig. 3), it varies from -36.0 to -42.9 km s<sup>-1</sup>. This difference is probably caused by a different inclination of the flow of ionized gas along the line of sight. Indeed, an examination of Figure 3 shows the southern bright rim edge-on and the northern one almost face-on.

To better illustrate this velocity gradient, the nebula was cut into eight sectors centered on the radio continuum maximum at 21 cm, which coincides in coordinates with the hot component of the molecular cloud. The mean value of every velocity point, having the same radius, has been calculated inside each sector. Plots of the LSR velocity versus the radius in arc minutes are shown in Figure 7 for each sector. The flow of ionized gas starting at the molecular cloud is clearly apparent

for sectors 5, 6, 7, and 8. The sectors numbered 1, 2, 3 intercept the molecular cloud, thus showing shorter plots and more

TABLE 2  
DEFINITION OF THE SYMBOLS USED  
IN THE VELOCITY FIELD MAPS

Symbol	Number of Points in a 1' Window
A .....	1
B .....	2-9
C .....	10-25
D .....	26-50
H .....	51-75
I .....	76-99
Z .....	>99

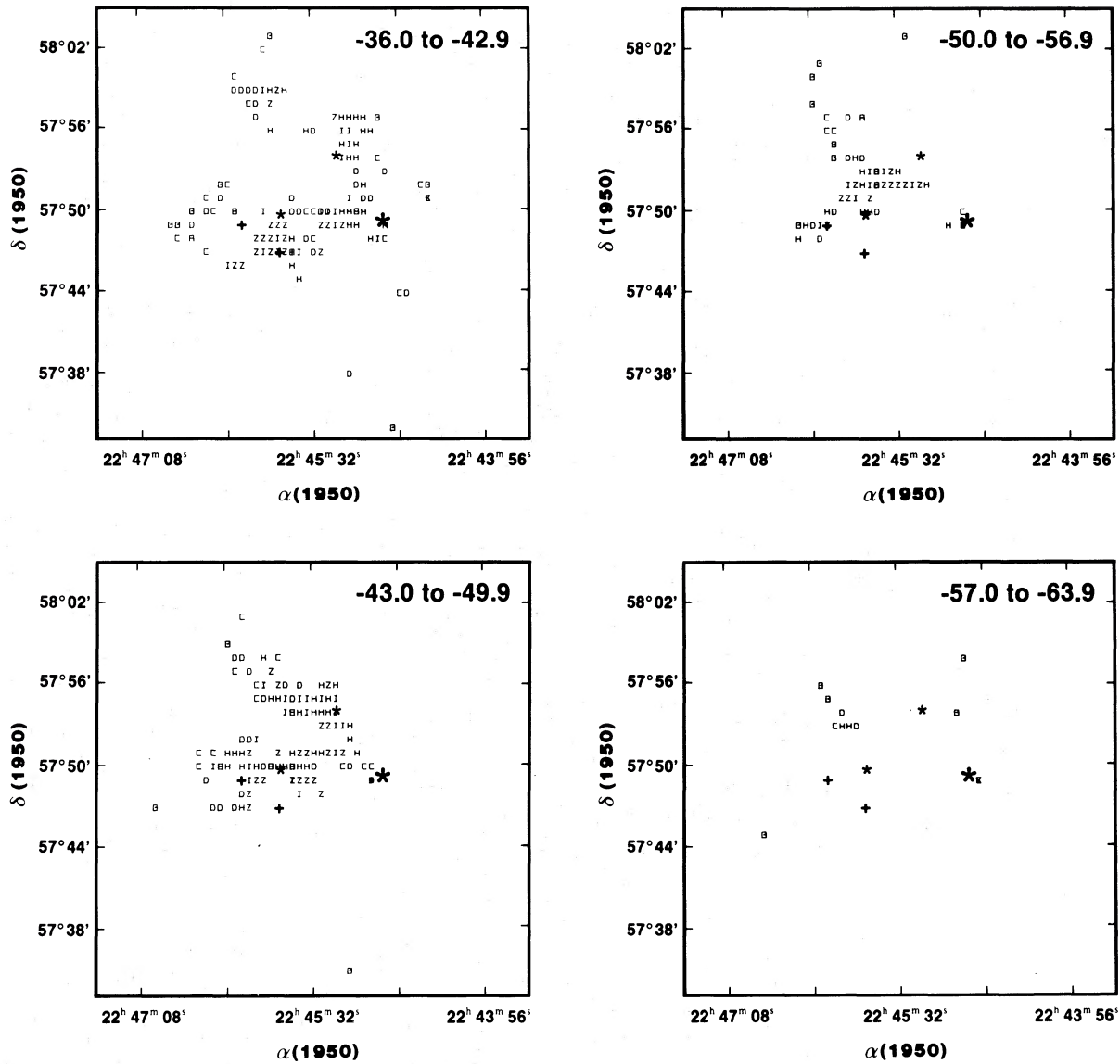


FIG. 5a—Continued

gentle slopes. Starting at  $-50 \text{ km s}^{-1}$ , their stopping points are  $\sim -40 \text{ km s}^{-1}$ , the LSR velocity of the molecular cloud. The mean gradient along the eight sectors is  $1.1 \text{ km s}^{-1} \text{ arcmin}^{-1}$  (i.e.,  $\sim 1 \text{ km s}^{-1}$  per projected pc). Thus the ionized gas found in the western part of S142 appears to flow away from the molecular cloud (and away from the observer) at a speed of  $\sim 35 \text{ km s}^{-1}$ , into the surrounding interstellar medium. No obvious correlation exists between the radial velocity field and any of the exciting stars.

On a graph (Fig. 8) of the LSR velocity versus the right ascension (compression along the declination axis) a small velocity gradient with respect to the molecular cloud is present. The scatter is large, however, and masks the presence of a systematic trend. A compression along the right ascension axis ( $V_{\text{LSR}}$  versus declination) is also shown in Figure 9. The highest negative velocities ( $\sim -50 \text{ km s}^{-1}$ ) are located at the declination of the hot component of the molecular cloud ( $57^\circ 51' 40''$ ). On either side of this inflection point, the velocities become less negative ( $\sim -18 \text{ km s}^{-1}$ ). There is a less conspicu-

ous inflection point further south, where velocities become more negative again ( $\sim -35 \text{ km s}^{-1}$ ). The ionized gas at this level may be close to an ionization front (IF). This is confirmed by the inspection of the 21 cm continuum radio map (Fig. 6). An intensity maximum is present in the southeastern part of S142, consistent with the presence of an IF. These ( $\alpha$ ,  $\delta$  versus  $V_{\text{LSR}}$ ) representations will be useful for comparison with similar spectral representation of 21 cm line observations of H I to be presented in a forthcoming paper.

### c) Velocity Dispersion in S142

Our large sample of velocity points allows us to do a meaningful analysis of the LSR velocity variations across S142. We calculated the standard deviation of the LSR velocities obtained from the average of all the velocity points inside each  $1' \times 1'$  window, provided that more than 10 velocity points were present in the window; we call this standard deviation "velocity dispersion." This velocity dispersion does not have the same exact meaning as the one deduced from line profiles, because

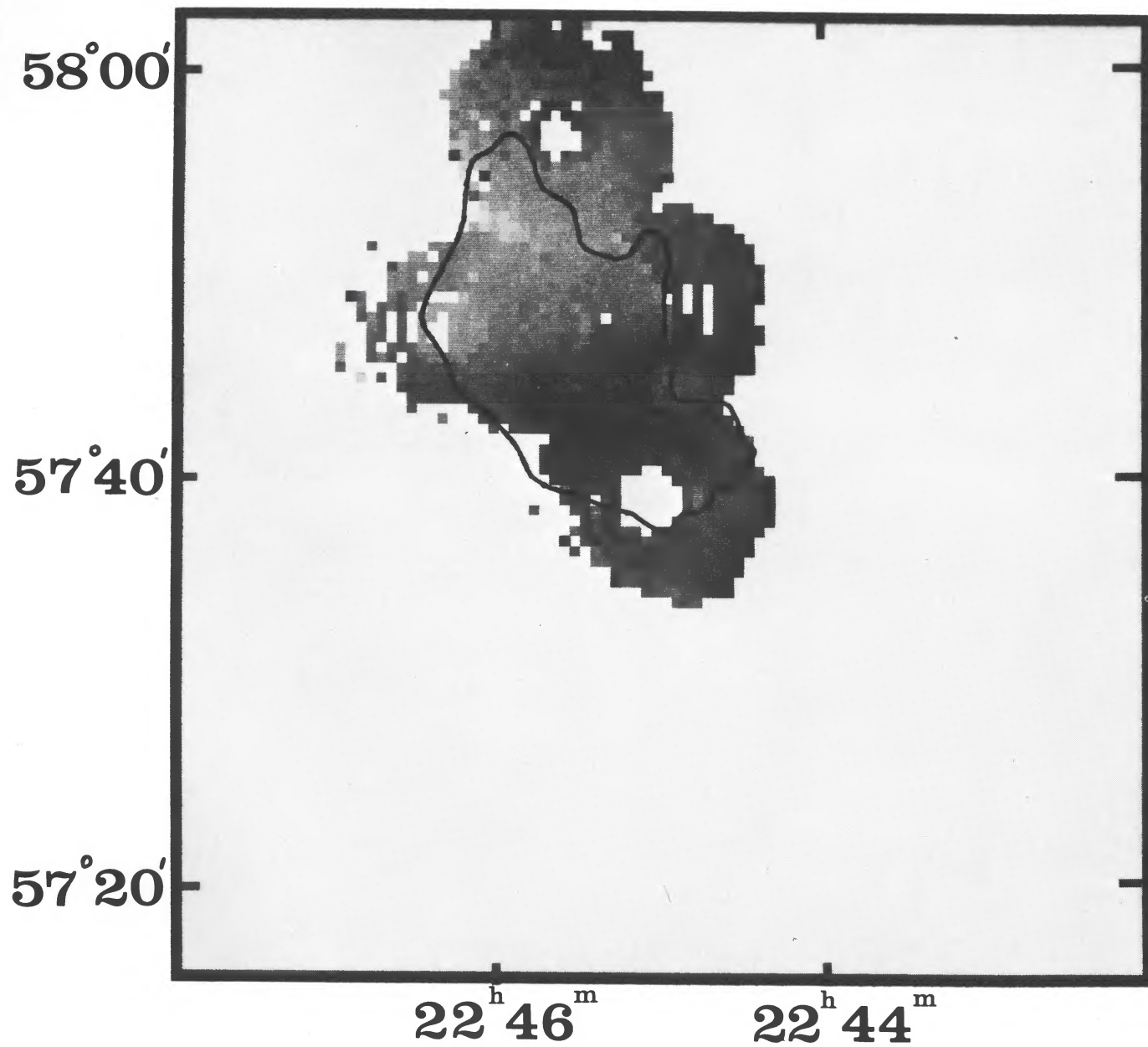


FIG. 5b

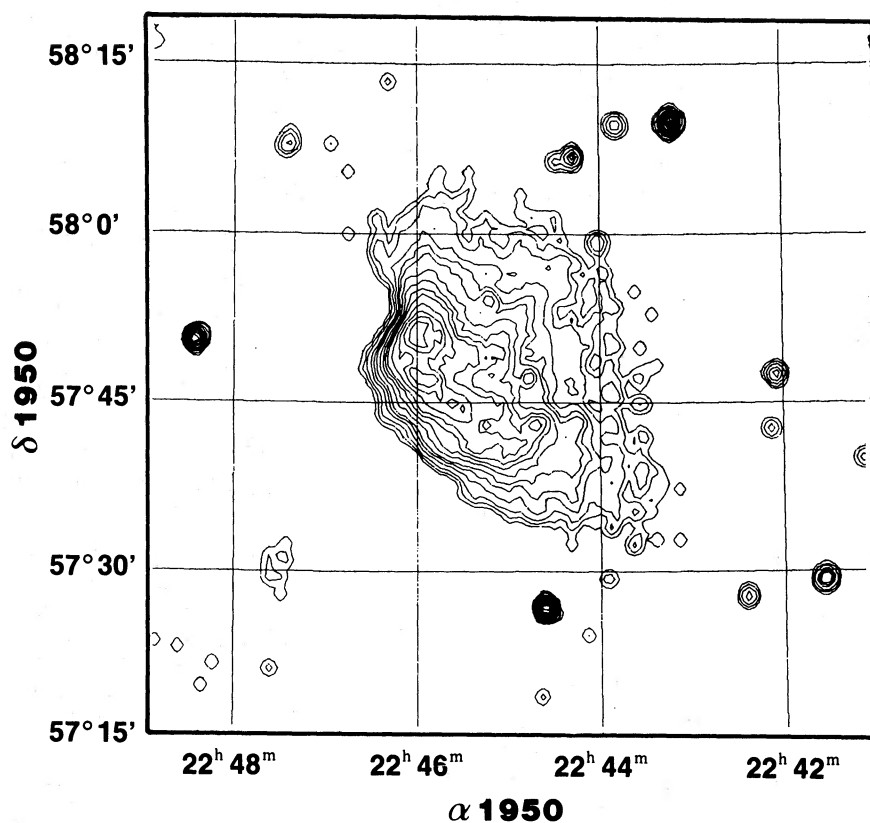


FIG. 6.—Radio continuum map of the ionized gas at 21 cm obtained at the Dominion Radio Astrophysical Observatory (Penticton) with a beam width of  $1' \times 1.2'$ . Notice the steep eastern gradient which corresponds to the  $H\alpha$  bright rims. The zones of the strongest emission also coincide with the *loci* of the most negative velocities (Fig. 5). Total flux from the region is about 12 Jy. Low order spacings (0, 1, 2, and 3) have not been included. Contours are 1, 2.5, 5, 10, 15, 20, 40, 50, 60, 80, 100, 120, and 140 mJy per synthesized beam.

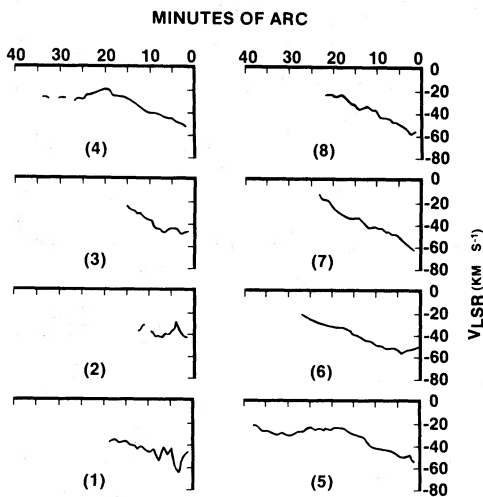


FIG. 7a

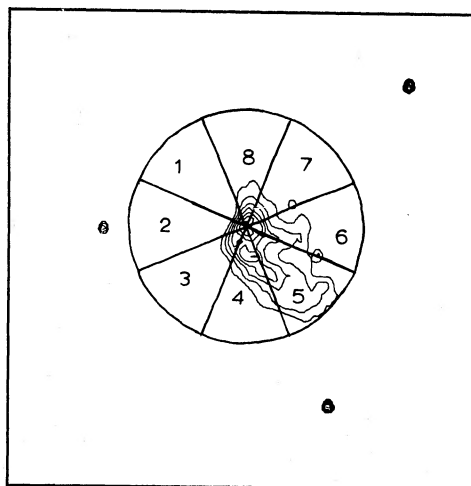


FIG. 7b

FIG. 7.—(a) Display of the velocity gradient inside eight sectors of the nebula centered at the point corresponding to the peak of 21 cm continuum emission. (b) Representation of the eight sectors defined for the display of the velocity gradient across S142. All radii are in arcmin.

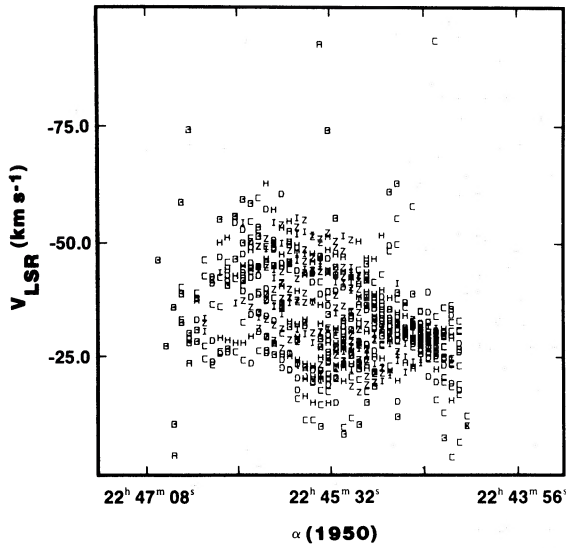


FIG. 8.—Compression along the declination axis of the integral H $\alpha$  velocity map produces this  $V_{\text{LSR}}$  versus  $\alpha(1950)$  “spectrum” of S142.

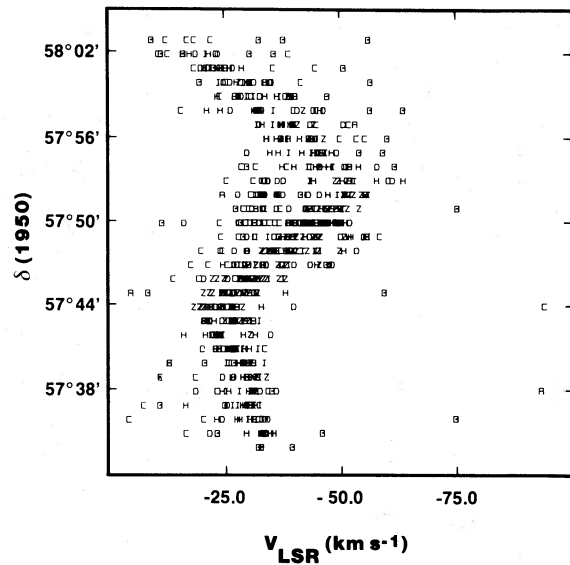


FIG. 9.—Compression along the right ascension axis of the integral H $\alpha$  velocity map produces the  $V_{\text{LSR}}$  versus  $\delta(1950)$  “spectrum” of S142.

our velocities are not weighted for the intensity of the measured points. Furthermore, most authors have measured the width of the turbulence broadening as the  $1/e$  width of the corresponding Gaussian; since the standard deviation measures the width at  $1/e^{1/2}$ , our values must be multiplied by  $2^{1/2}$ . The histogram of the velocity dispersion for a  $1' \times 1'$  grid over S142 is shown in Figure 10. The mean value of the velocity dispersion is  $9.8 \text{ km s}^{-1}$  with a new standard deviation of  $5.6 \text{ km s}^{-1}$ ; the most probable velocity dispersion is  $7.0 \pm 0.2 \text{ km s}^{-1}$ . This histogram tells us that an F-P spectrometer with a  $1'$  diaphragm would measure H $\alpha$  line profiles with a  $2^{1/2} \times 7 \text{ km s}^{-1} \approx 10 \text{ km s}^{-1}$ , average turbulence broadening. The skewness of the histogram is  $-0.92$ . Not too surprisingly, this value of  $7.0 \pm 0.2 \text{ km s}^{-1}$  is smaller than the value of  $12.5 \pm 0.1 \text{ km s}^{-1}$  of the complete histogram. Using a  $1'$  window, we are more likely to sample the small-scale velocity field, because little weight is given to the systematic large-scale movements such as the expansion described in the preceding section.

Velocity dispersion maps (Fig. 11), for a  $1' \times 1'$  grid, were drawn with a step of  $5 \text{ km s}^{-1}$  to search for any correlations with particular nebular features (symbols are those of Table 2). There is no systematic trend of velocity dispersion across the nebula; the dispersion is not larger near the bright rims, nor close to the O9 star located in the eastern part of the nebula. Instead, the highest dispersions ( $\geq 20 \text{ km s}^{-1}$ ) appear in the western section of S142 and close to the main exciting star HD 215835. A first possible interpretation may be the interaction between the H II region and a hot bubble created by a stellar wind coming from the star. Another one is that the downstream flow of ionized gas originating at the molecular cloud becomes more turbulent; but if this effect exists, it is marginally visible in S142. For the remaining parts of the nebula, there does not seem to be any obvious correlation between features of S142 and its velocity dispersion field; this may reflect the relatively old age of the nebula.

V. DISCUSSION

There are many more or less direct pieces of evidence that S142 is relatively old, i.e., of age greater than  $10^6$  years. First, the cluster NGC 7380, to which the main exciting star belongs,

is aged 2 to  $3 \times 10^6$  years (Moffat 1971). No star-forming activity, as would be indicated by the presence of masers or infrared sources, is presently taking place in or close to S142. S142 is a large region ( $d \approx 25 \text{ pc}$ ) of low mean electronic density ( $n \approx 20 \text{ cm}^{-3}$ ). The main exciting star is away from the area of maximum H $\alpha$  and 21 cm continuum emission, at about 15 projected parsecs from the eastern photon-bounded side of the nebula; assuming an average penetration speed of  $10 \text{ km s}^{-1}$  into the neutral cloud, a kinematic age greater than  $10^6$  years is implied. Furthermore, the size ( $d_{\text{CO}} = 7 \text{ pc}$ ), the mass ( $M_{\text{CO}} = 200 M_{\odot}$ ), and the density ( $N_{\text{CO}} = 60 \text{ cm}^{-3}$ ) of the associated molecular cloud are small, suggesting that evaporation has been disrupting the cloud for quite some time. The amount of ionized gas in the nebula  $M_{\text{HII}} = 4/3\pi N_{\text{HII}} m_{\text{H}} r_{\text{HII}}^3$  corresponds to about  $2000 M_{\odot}$ . From the observed flow near the molecular cloud, one can calculate the rate at which neutral material is

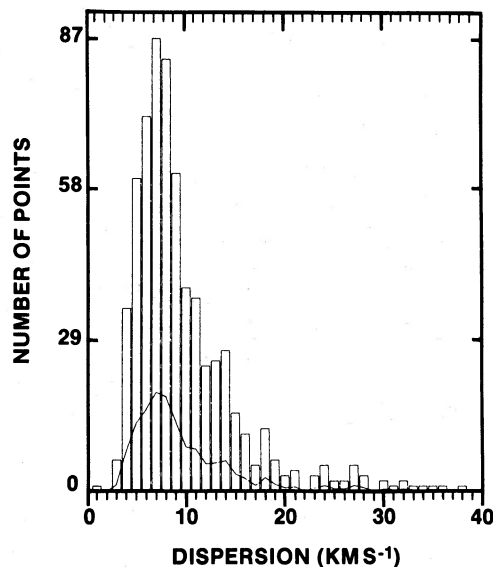


FIG. 10.—Histogram of the velocity dispersion across S142.

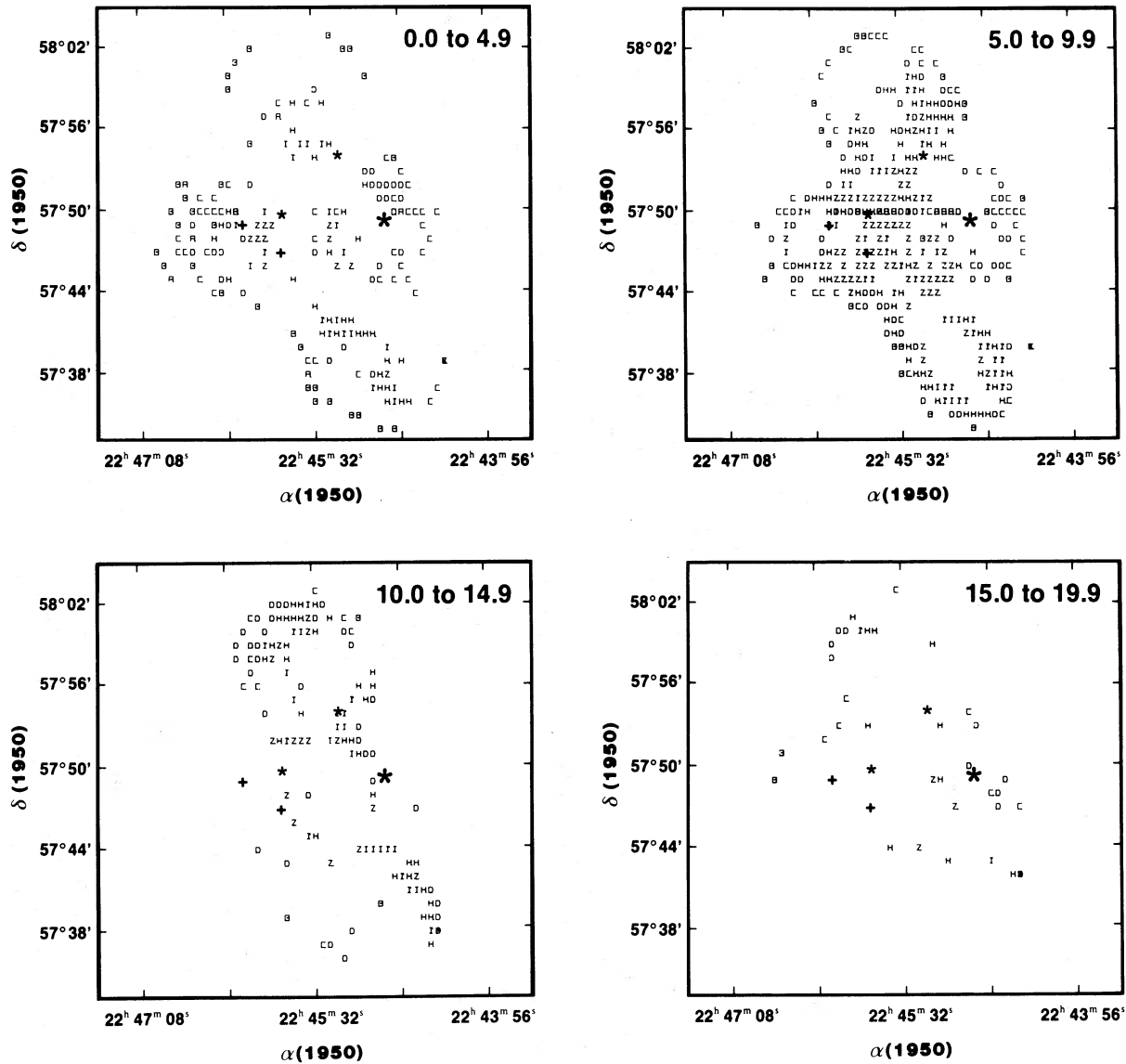


FIG. 11.—Maps of H $\alpha$  LSR velocity dispersion in step of  $5 \text{ km s}^{-1}$  for a  $1' \times 1'$  mesh. Symbols are the same as in Fig. 5a.

being evaporated as  $\dot{M}_{\text{HII}} = \rho_{\text{HII}} V_{\text{HII}} \pi r_{\text{CO}}^2$ . The observed H $\alpha$  velocities close to the molecular cloud are  $\sim -10^6 \text{ cm s}^{-1}$ , and the increased H $\alpha$  brightness indicates that the density is higher there than for the average nebula. For  $\rho_{\text{HII}} = 2 \times 10^{-22} \text{ g cm}^{-3}$  ( $N \approx 100 \text{ cm}^{-3}$ ) and  $r_{\text{CO}} \approx 10^{19} \text{ cm}$ ,  $\dot{M} \approx 10^{-3} M_{\odot} \text{ yr}^{-1}$  leading to an evaporation age  $2 \times 10^6$  years to account for the present amount of ionized gas in S142.

The most successful model describing the formation and the evolution of an H II region has been the “champagne” model proposed by Tenorio-Tagle (1979). Its success with respect to the classical approach (e.g., Spitzer 1968) is to be able to reproduce many aspects of the morphology and velocity structure of nebulae, in particular the large terminal supersonic velocities.

Considering the evolved stage of S142, it appears at first somewhat surprising that many details of the velocity structure that we measured across S142 are qualitatively and quantitatively consistent with the champagne model; for example, case 1 discussed by Bodenheimer, Tenorio-Tagle, and Yorke (1979,

Fig. 2f) represents very well the kinematics of S142. The calculated velocity field seen edge-on resembles the observed one for S142, except that the theoretical age is at least 4 times less than the inferred age of S142. One could believe that the model, which describes the sudden emptying of the high-pressure H II pocket of ionized gas piercing the edge of the parent molecular cloud to undergo free expansion into the low-pressure intercloud medium, is restricted to a brief period of time of  $\sim 10^5$  years. But this is not necessarily the case. The champagne phase, once started, should continue to operate for as long as a cloud phase is present. This is simply due to the fact that upon ionization, the high-density cloud material will have a larger pressure than surrounding gas; this pressure gradient is able to maintain the champagne flow. Indeed, recent calculations of champagne flows by Yorke, Tenorio-Tagle, and Bodenheimer (1983) have been extended to more than  $4 \times 10^6$  years. The persistence of the champagne flow emphasizes the role played by the ionization-induced pressure gradient in maintaining the

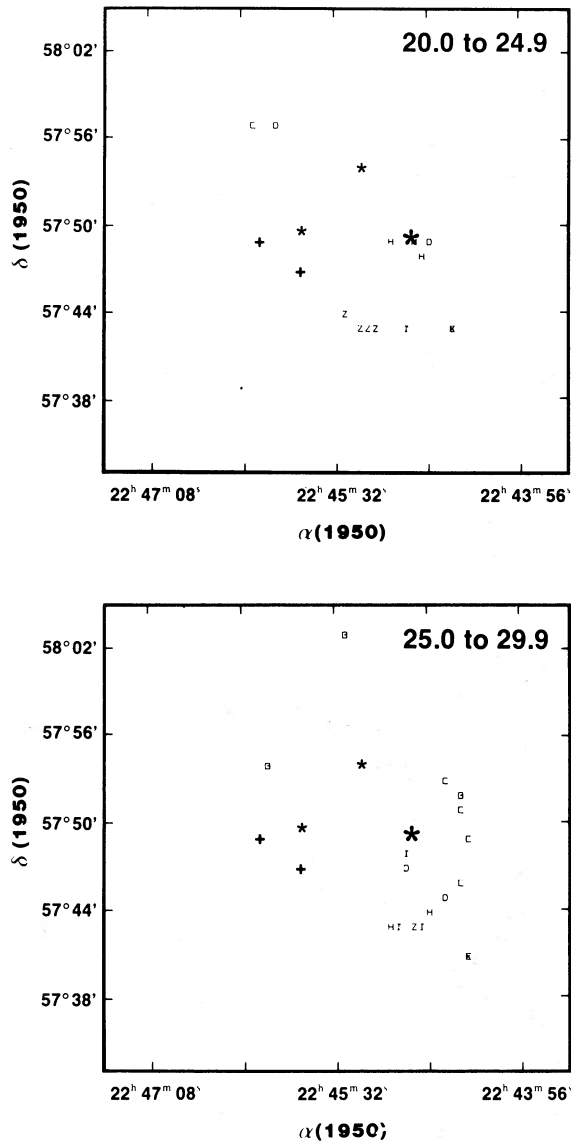


FIG. 11—Continued

champagne phase for as long as there is a neutral cloud to dissociate.

We summarize the observational evidences favoring the application of the champagne model to the H II region S142:

1. S142 is associated with a molecular cloud. Although the associated molecular cloud is much smaller in size and in mass than the H II region and its density low ( $60 \text{ cm}^{-3}$ ), the latter is probably sufficient to provide a density ratio with the intercloud medium high enough to power the champagne flow.

2. There is general agreement between the observed and the predicted velocity field across the nebula: the  $1 \text{ km s}^{-1} \text{ pc}^{-1}$  velocity gradient from the ionization-bounded side to the density-bounded side, the terminal velocities of  $\sim 35 \text{ km s}^{-1}$ , and the  $7 \text{ km s}^{-1}$  velocity at which the ionized material appears to be streaming away from the neutral cloud. The density of the ionized gas decreases in the direction where the velocity increases.

3. DH Cep, the main exciting star, does not occupy a special position in the velocity field, nor do the two other O stars.

4. There is agreement between the observed and theoretical radio continuum maps of an H II region in the champagne phase (e.g., compare our Fig. 6 with Yorke, Tenorio-Tagle, and Bodenheimer 1983, Fig. 1).

Finally, some other possibilities should be explored. For example, DH Cep could be a runaway star which has encountered a dense neutral cloud; the H II region would be the product of straight evaporation resulting from the encounter. This appears unlikely, however, because the radial velocity of DH Cep ( $V_{\text{LSR}} = -28 \text{ km s}^{-1}$ ) does not indicate a straggling nature, unless a large velocity component is hidden in the plane of the sky. Moreover, the velocity field, the density, and the morphology predicted for an H II region generated in such a way (Tenorio-Tagle, Yorke, and Bodenheimer 1979) are strikingly different from those observed in S142. On the other hand, some extraneous driving mechanism could also power the champagne flow well beyond the time taken by the original shower to subside. Sandford, Whitaker, and Klein (1982) have shown that jets of ionized gas moving into the intercloud medium with velocities of the order of  $25 \text{ km s}^{-1}$  can be produced by the interaction of the radiation-driven ionization shock fronts with the geometrically inhomogeneous molecular cloud; such interface inhomogeneities could be present along the eastern edge of S142. Another lasting input of mechanical energy could come from the expanding bubbles generated by the stellar winds produced by the O6 binary star DH Cep (Weaver *et al.* 1977). A detailed discussion of these mechanisms is beyond the scope of this paper.

## V. CONCLUSION

The use of an efficient Fabry-Pérot interferometer camera and the application of image processing techniques have allowed us to measure close to 41,000 velocity points across the H II region S142. This extensive sampling has led to the most detailed velocity map of an H II region to this date. S142 and most of its associated neutral complex seem to be seen mostly edge-on. The locus of the most negative H $\alpha$  velocities ( $\sim -50 \text{ km s}^{-1}$ ) coincides with the position of the "hot" component of the CO molecular cloud east of the nebula. The observed velocity field is readily explained as a systematic expansion of the ionized gas away from the molecular cloud and from the observer. At the bright H $\alpha$  rims, the ionized gas is observed to be streaming away from the neutral cloud at a velocity of about  $-10 \text{ km s}^{-1}$ . There is indeed a striking match between the most negative velocities and the shape of the CO emission contours. Some neutral material, especially in the northeastern section, is probably located behind the H II region while some more acts as a wall across the face of the H II region, inhibiting the flow of ionized gas in our direction. Consequently, we observe a flow apparently directed westward (away from the molecular cloud) and away from us. This flow configuration explains the radial velocity gradient across the nebula and the fact that the mean  $V_{\text{LSR}}$  for the whole nebula is redshifted by  $+5 \text{ km s}^{-1}$  with respect to the  $-41 \text{ km s}^{-1}$  of the molecular cloud. (We do not accept the CO cloud being in front of the nebula as a defensible alternative.) The terminal velocities measured at the western periphery reach about  $35 \text{ km s}^{-1}$  with respect to the  $V_{\text{LSR}}$  of the molecular cloud. Several features of the observed kinematics and of the optical and radio morphology of S142 agree with the prediction of the champagne flow. In particular, we have detected the largest streaming velocities predicted by the champagne model.

We are grateful to numerous colleagues who provided suggestions and stimulating discussions throughout this project. We thank in particular L. Higgs, Y. Georgelin, G. Tenorio-Tagle, E. Hardy, P. Dewdney, R. Arsenault, D. Durand, and S. Pineault. B. Malenfant and G. Turcotte were our faithful night

assistants at the Observatoire astronomique du mont Mégantic. C. Beaulieu helped in preparing the manuscript.

The National Science and Engineering Research Council of Canada and the FOND FCAC of Quebec provided funds to support this research project.

## REFERENCES

- Andrews, P. J. 1968, *Mem. R.A.S.*, **72**, 35.  
 Atherton, P. D., Taylor, K., Pike, C. D., Harmer, C. F. W., Parker, N. M., and Hook, R. N. 1982, *M.N.R.A.S.*, **201**, 661.  
 Blitz, L., Fich, M., and Stark, A. A. 1982, *Ap. J. Suppl.*, **49**, 183.  
 Bodenheimer, P., Tenorio-Tagle, G., and Yorke, H. W. 1979, *Ap. J.*, **233**, 85.  
 Born, M., and Wolf, E. 1975, *Principles of Optics* (New York: Pergamon).  
 Chopinet, M., and Lortet-Zuckermann, M. C. 1972, *Astr. Ap.*, **18**, 373.  
 Courtès, G. 1972, *Vistas in Astronomy*, **14**, 81.  
 Courtès, G., Cruvellier, P., Georgelin, Y. P., and Astier, N. 1966, *J. Observateurs*, **49**, 329.  
 Crampton, D., Georgelin, Y. M., and Georgelin, Y. P. 1978, *Astr. Ap.*, **66**, 1.  
 Deharveng, L. 1980, Thèse de doctorat d'état, Université d'Aix-Marseille I.  
 Felli, M., and Harten, R. H. 1981, *Astr. Ap.*, **100**, 28.  
 Felli, M., Harten, R. H., Habing, H. J., and Israel, F. P. 1978, *Astr. Ap. Suppl.*, **32**, 423.  
 Felli, M., Toffani, G., Fanti, C., and Tomasi, P. 1977, *Astr. Ap. Suppl.*, **27**, 181.  
 Fountain, W. F., Gary, G. A., and O'Dell, C. R. 1979, *Ap. J.*, **229**, 971; Erratum *Ap. J.*, **236**, 1056.  
 ———. 1983, *Ap. J.*, **269**, 164.  
 Garay, G., and Rodriguez, L. F. 1983, *Ap. J.*, **266**, 263.  
 Georgelin, Y. P., and Georgelin, Y. M. 1970, *Astr. Ap.*, **6**, 349.  
 Goy, G. 1973, *Astr. Ap. Suppl.*, **12**, 277.  
 Hawley, S. A. 1978, *Ap. J.*, **224**, 417.  
 Hiltner, W. A. 1956, *Ap. J. Suppl.*, **2**, 389.  
 Humphreys, R. M. 1978, *Ap. J. Suppl.*, **38**, 309.  
 Israel, F. P. 1977, *Astr. Ap.*, **60**, 233.  
 Israel, F. P. 1978, *Astr. Ap.*, **70**, 769.  
 ———. 1980, *A.J.*, **85**, 1612.  
 Joncas, G. 1983, Ph.D. thesis, Université Laval.  
 Joncas, G., and Roy, J.-R. 1984, *Pub. A.S.P.*, **96**, 263.  
 Lang, K. R. 1980, *Astrophysical Formulae* (New York: Springer), p. 535.  
 Miller, J. S. 1968, *Ap. J.*, **151**, 473.  
 Miller, W. C. 1978, *Observatory Photographic Manual* (Pasadena: Hale Observatories).  
 Moffat, A. F. J. 1971, *Astr. Ap.*, **13**, 30.  
 Mufson, S. L., Fountain, W. F., Gary, G. A., Howard, W. E., III, O'Dell, C. R., and Wolff, T. M. 1981, *Ap. J.*, **248**, 992.  
 Panagia, N. 1973, *A.J.*, **78**, 929.  
 Pedlar, A., 1980, *M.N.R.A.S.*, **192**, 179.  
 Pottach, S. R. 1958, *Bull. Astr. Inst. Netherlands*, **14**, 29.  
 Sandford, M. J., II, Whitaker, R. W., and Klein, R. I. 1982, *Ap. J.*, **260**, 183.  
 Spitzer, L. 1968, in *Star and Stellar Systems*, Vol. 7, ed. B. M. Middlehurst and L. H. Aller (Chicago: University of Chicago Press), p. 1.  
 Tenorio-Tagle, G. 1979, *Astr. Ap.*, **71**, 59.  
 Tenorio-Tagle, G., Yorke, H. W., and Bodenheimer, P. 1979, *Astr. Ap.*, **80**, 110.  
 Weaver, R., McCray, R., Castor, Shapiro, P., and Moore, R. 1977, *Ap. J.*, **218**, 377.  
 Williamson, R. A. 1970, *Ap. Space Sci.*, **6**, 45.  
 Wilson, O. C., Münch, G., Flather, E. M., and Coffeen, M. F. 1959, *Ap. J. Suppl.*, **4**, 199.  
 Yorke, H. W., Tenorio-Tagle, G., and Bodenheimer, P. 1983, *Astr. Ap.*, **127**, 313.

GILLES JONCAS: Observatoire de Marseille, 2 Place Le Verrier, 13248 Marseille, France

JEAN-RENÉ ROY: Département de physique, Université Laval, Québec, QC G1K 7P4, Canada